Mon. Not. R. Astron. Soc. **000**, 1–10 (2002) Printed 6 June 2014 (MN LATEX style file v2.2)

Frequencies and resonances around L_4 in the elliptic restricted three-body problem

R. Rajnai[1⋆], I. Nagy[2], B. Érdi[3]
[1] *Department of Mathematics and Computational Sciences, Széchenyi University, Egyetem tér 1, H-9026 Győr, Hungary*
[2] *Department of Science, National University of Public Service, Hungária körút 9-11, H-1101 Budapest, Hungary*
[3] *Department of Astronomy, Eötvös University, Pázmány Péter sétány 1/A, H-1117 Budapest, Hungary*

arXiv:1406.1331v1 [astro-ph.EP] 5 Jun 2014

date

ABSTRACT

The stability of the Lagrangian point L_4 is investigated in the elliptic restricted three-body problem by using Floquet's theory. Stable and unstable domains are determined in the parameter plane of the mass parameter and the eccentricity by computing the characteristic exponents. Frequencies of motion around L_4 have been determined both in the stable and unstable domains and fitting functions for the frequencies are derived depending on the mass parameter and the eccentricity. Resonances between the frequencies are studied in the whole parameter plane. It is shown that the 1:1 resonances are not restricted only to single curves but extend to the whole unstable domain. In the unstable domains longer escape times of the test particle from the neighbourhood of L_4 are related to certain resonances, but changing the parameters the same resonances may lead to faster escape.

Key words:
celestial mechanics, – methods: analytical, numerical, – planets and satellites: dynamical evolution and stability

1 INTRODUCTION

The elliptic restricted three-body problem (ERTBP) is a thoroughly investigated problem of celestial mechanics which has received continuing attention for a long time, due to its theoretical interest and practical applicability in the dynamics of planetary systems. In the ERTBP a basic question is the stability of the Lagrangian triangular equilibrium point L_4. Since the ERTBP has two free parameters, the mass ratio μ and the orbital eccentricity e of the primaries, and the linear variational equations of motion around L_4, determining stability or instability, have periodic coefficients, the problem is more difficult than in the circular restricted three-body problem, with the only parameter μ and constant coefficients of the variational equations.

Floquet's theory (Floquet 1883) of differential equations with periodic coefficients was used by Danby (1964) to determine the boundaries of the stable domain of L_4 in the μ, e plane, and by Bennett (1965) to describe the structure of the unstable domain. Rabe (1973) derived an algebraic equation from which the four frequencies of libration around L_4 in the ERTBP can be computed for small values of e. Transition curves, separating stable and unstable domains, were determined by analytical (Tschauner 1971) and numerical (Meire 1981) methods.

Non-linear stability of L_4 and the extension of the stable region around L_4 in the configuration plane, depending on μ and e, were studied numerically by Lohinger & Dvorak (1993) and also by Markellos, Papadakis & Perdios (1995) who showed the shrinking of the stable region around L_4 at certain combinations of μ and e corresponding to unstable resonances. Types of resonances between the frequencies of libration in the ERTBP were defined in Érdi et al. (2007) and their connection with the minima of the size of the stable region were studied in detail in Érdi et al. (2007, 2009). Applications to possible Trojan exoplanets were investigated in Schwarz et al. (2012). Recently, by using Hill's equation and the energy-rate method, Kovács (2013) pointed out the dominant role of the long-period component of libration in forming the structure of the stability domain of L_4.

In this paper we study the resonances between the frequencies of motion around L_4 in the ERTBP in a larger domain of the μ, e parameter plane than before (Érdi et al. 2007, 2009), giving a more extended view on the relation between resonances and the structure of the stable and unstable domains of L_4.

The paper is organized as follows. The equations of motion are given and the applied methods are described in

⋆ E-mail: rajnair@sze.hu

Section 2. Characteristic roots and characteristic exponents are discussed in Section 3. Comparison of the frequencies obtained by Floquet's theory and fast Fourier transformation is made in Section 4, where fitting functions for the frequencies are also determined. Resonances between the frequencies and their connection with the structure of the stable and unstable domains are studied in Section 5. Conclusions are drawn in Section 6. The Appendix gives the fitting functions and their coefficients for the frequencies.

2 MODEL AND METHOD

2.1 Equations of motion

The ERTBP studies the motion of a point-like body with negligible mass (in the following a test particle), moving in the orbital plane and under the gravitational influence of two point-like massive bodies (the primaries), which revolve around their barycentre in elliptic orbits. The equations of motion of the test particle, in a barycentric coordinate system, rotating together with the primaries with the x-axis going through them, are (Szebehely 1967)

$$x'' - 2y' = \alpha\frac{\partial\Omega}{\partial x}, \quad y'' + 2x' = \alpha\frac{\partial\Omega}{\partial y}, \tag{1}$$

where x and y are the rectangular coordinates of the test particle, the prime means derivation according to the true anomaly v of the primaries, serving as independent variable,

$$\alpha = \frac{1}{1+e\cos v},$$

and e is the eccentricity of the relative orbit of the primaries.

The potential function Ω is

$$\Omega = \frac{1}{2}\left[(1-\mu)r_1^2 + \mu r_2^2\right] + \frac{1-\mu}{r_1} + \frac{\mu}{r_2},$$

where μ is the mass parameter

$$\mu = \frac{m_2}{m_1+m_2},$$

m_1 and m_2 being the masses of the primaries, and r_1, r_2 are the distances of the test particle from the primaries

$$r_1 = \sqrt{(x-\mu)^2+y^2}, \quad r_2 = \sqrt{(x+1-\mu)^2+y^2}.$$

The coordinates and distances are dimensionless, the instantaneous distance between the primaries serving as distance unit (the equations of motion are written in the so-called rotating 'pulsating' coordinate system). The ERTBP depends on two parameters, the eccentricity $0 \leqslant e < 1$, and the mass parameter $0 < \mu \leqslant 0.5$.

The equations of motion have five equilibrium solutions, the Lagrangian points L_i. The linear stability of these points can be studied by using the first variational equations of motion

$$\begin{pmatrix} \xi' \\ \eta' \\ \xi'' \\ \eta'' \end{pmatrix} = \begin{pmatrix} 0 & 0 & 1 & 0 \\ 0 & 0 & 0 & 1 \\ \alpha\,\Omega_{xx}^{(i)} & \alpha\,\Omega_{xy}^{(i)} & 0 & 2 \\ \alpha\,\Omega_{xy}^{(i)} & \alpha\,\Omega_{yy}^{(i)} & -2 & 0 \end{pmatrix} \begin{pmatrix} \xi \\ \eta \\ \xi' \\ \eta' \end{pmatrix}, \tag{2}$$

where ξ, η, ξ', η' are infinitesimal displacements in the position and velocity coordinates of L_i, and the partial derivatives of Ω have to be computed at the points L_i. Specifically, $\Omega_{xx}^{(4)} = 3/4$, $\Omega_{xy}^{(4)} = \frac{3\sqrt{3}}{2}(\mu - 1/2)$, $\Omega_{yy}^{(4)} = 9/4$ for the triangular Lagrangian point L_4.

For $e = 0$, the system (1) gets simplified to the circular restricted three-body problem, for which Eqs (2) make up a linear system of differential equations with constant coefficients. For $e > 0$, (2) is a linear system of differential equations with periodic coefficients (of period 2π) that can be studied by using Floquet's theory (Floquet 1883).

2.2 Floquet's theory

For convenience, here we repeat Floquet's theory, following the scenario described by Danby (1964) and Bennett (1965), based on Floquet (1883).

By defining the new variables $x_1 = \xi$, $x_2 = \eta$, $x_3 = \xi'$, $x_4 = \eta'$, (2) can be written in the compact form

$$\mathbf{x}' = \mathbf{A}(t)\mathbf{x}\ , \tag{3}$$

where $\mathbf{x} = (x_1, x_2, x_3, x_4)^T$ (the upper index ^{T} denoting the transpose of a matrix), and $\mathbf{A}$ is the coefficient matrix in (2).

Let $\mathbf{x}^1, \ldots, \mathbf{x}^4$ be 4 linearly independent solutions of (3), then

$$\mathbf{X}(t) = \begin{pmatrix} \mathbf{x}^1 & \mathbf{x}^2 & \mathbf{x}^3 & \mathbf{x}^4 \end{pmatrix} \tag{4}$$

is called a fundamental matrix, satisfying $\mathbf{X}'(t) = \mathbf{A}(t)\mathbf{X}(t)$.

Floquet's theorem (Floquet 1883) states, that if $\mathbf{X}(t)$ is a fundamental matrix solution of the system (3) with periodic coefficients of period T, then so is $\mathbf{X}(t+T)$, and there exists a non-singular constant matrix $\mathbf{B}$, such that $\mathbf{X}(t+T) = \mathbf{X}(t)\mathbf{B}$ for all t. According to this, if $\mathbf{X}(t)$ is such a solution that at $t = t_0$, $\mathbf{X}(t_0) = \mathbf{I}$ where $\mathbf{I}$ is the identity matrix, then

$$\mathbf{X}(t_0 + T) = \mathbf{B}. \tag{5}$$

The eigenvalues λ_j of $\mathbf{B}$ ($j = 1, 2, 3, 4$) are the characteristic roots of the system (3). They are an intrinsic property of the system, and independent of the choice of the fundamental matrix.

The characteristic exponents ν_j are defined by

$$\lambda_j = \exp(\nu_j T), \quad j = 1, 2, 3, 4. \tag{6}$$

Writing λ_j in the form $\lambda_j = |\lambda_j| \cdot \exp(i\varphi_j)$, the characteristic exponents ν_j can be obtained from the characteristic roots λ_j as

$$\nu_j = \frac{\ln|\lambda_j|}{T} + i\left(\frac{\varphi_j + k2\pi}{T}\right), \quad k = 0, \pm1, \pm2, \ldots, \tag{7}$$

that is within a multiple of $2\pi i/T$.

The consequence of Floquet's theorem is that there exist 4 linearly independent solutions for (3) of the form

$$\mathrm{x}_j(t) = \exp(\nu_j t)p_j(t), \quad j = 1, 2, 3, 4, \tag{8}$$

where $p_j(t)$ is a periodic function with period T.

2.3 Applying Floquet's theory

Applying Floquet's theory to study the stability of L_4, we integrated numerically Eqs (2) for a period of the primaries, $T = 2\pi$, with 4 different initial conditions at $t = t_0$:

$$\begin{pmatrix} x_1 \\ x_2 \\ x_3 \\ x_4 \end{pmatrix} = \begin{pmatrix} 1 \\ 0 \\ 0 \\ 0 \end{pmatrix}, \begin{pmatrix} 0 \\ 1 \\ 0 \\ 0 \end{pmatrix}, \begin{pmatrix} 0 \\ 0 \\ 1 \\ 0 \end{pmatrix}, \begin{pmatrix} 0 \\ 0 \\ 0 \\ 1 \end{pmatrix}.$$

Thus $\mathbf{X}(t_0) = \mathbf{I}$. After one period, from the results of the numerical integration we could build up the matrix $\mathbf{B}$. Then we determined the characteristic roots λ_j and exponents ν_j of the system by using GNU Octave's built in functions.

We integrated Eqs (2) by changing the two parameters μ and e in the regions $0 < \mu \leqslant 0.5$, and $0 \leqslant e < 1$, with stepsize $\Delta\mu = 0.0001$, $\Delta e = 0.005$, thus we determined the characteristic roots and exponents for the whole μ, e parameter plane.

3 CHARACTERISTIC ROOTS AND EXPONENTS

3.1 Stability

The types of the characteristic roots λ_j determine the linear stability of L_4. It can be shown that the characteristic roots occur in reciprocal pairs (due to the fact that the equations of motion of the ERTBP can also be written in Hamiltonian form). Therefore, a pair of real roots λ_j and $1/\lambda_j$ always means instability, since either $|\lambda_j| > 1$ or $1/|\lambda_j| > 1$ and one solution (8) becomes unbounded. Since the equation for the eigenvalues of the matrix $\mathbf{B}$ has real coefficients, complex characteristic roots appear in reciprocal and conjugate pairs. Thus in the case of complex characteristic roots, stability holds only if all roots have unit modulus $|\lambda_j| = 1$, that is they are on the unit circle (otherwise $|\lambda_j| > 1$ or $1/|\lambda_j| > 1$ would make the solution unbounded).

We computed the characteristic roots depending on μ and e. According to their types, 4 regions can be distinguished in the μ, e plane as shown in the top panel of Fig. 1 for $\mu < 0.1$. This is in agreement with the results of Bennett (1965). L_4 is stable and stable periodic motion around it is only possible in the domain of 4 complex roots of unit modulus (S1 and S2 regions). The shape of the stability domain is well-known from previous investigations (Danby 1964; Érdi et al. 2007). Three critical points are associated with this region; two on the $e = 0$ axis at $\mu = 0.02859$ (point A in Fig. 1), dividing the stability domain for two parts, and at $\mu = 0.03852$ (point B), limiting the stability domain on the μ-axis, and a third at $e = 0.3143$, $\mu = 0.04698$ (point D) at the upper right peak of the stability domain.

L_4 is unstable in three domains (marked by U1, U2, and U3 in the top panel of Fig. 1), with characteristic roots of different properties. There are 2 real roots and 2 complex roots of unit modulus in the U1 domain, 4 complex roots of non-unit modulus in U2, and 4 real roots in U3. The U2 and U3 domains extend up to $\mu = 0.5$, the border between them approaching to $e = 1$ (not shown in Fig. 1).

The bottom panel of Fig. 1 shows the types of the characteristic exponents ν_j in the μ, e plane. In the stable domain, there are 4 purely imaginary exponents corresponding to the 4 complex characteristic roots of unit modulus in the S1, S2 domains. To the characteristic roots in the U1 domain, there correspond 2 complex and 2 imaginary exponents in the bottom panel of Fig. 1. The boundary between the U2 and U3 domains on the top panel vanishes in the bottom panel, since the 4 real characteristic roots are all negative and 4 complex exponents correspond to them, as well as to the roots in the U2 domain. However, the complex exponents corresponding to the roots in the U3 domain have equal imaginary parts, while the exponents corresponding to the roots in the U2 domain have two pairs of equal imaginary parts.

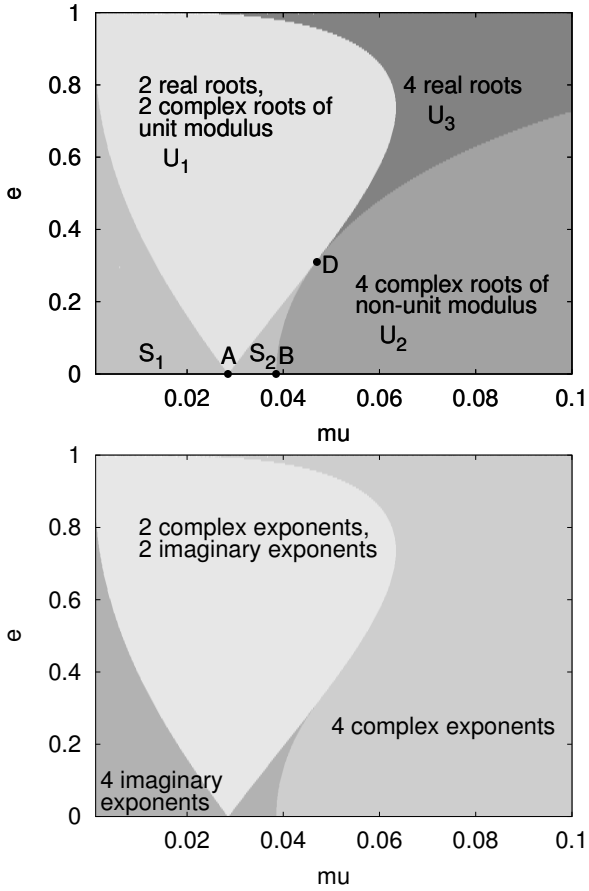

Figure 1. The types of the characteristic roots (top panel) and characteristic exponents (bottom panel) of the first variational equations, depending on μ and e. In the S1 and S2 regions (upper panel) there are 4 complex roots of unit modulus and L_4 is stable.

Moving away from the boundary of the stable domain (S1, S2), with increasing the eccentricity or the mass parameter, the characteristic roots slowly drift away from the unit circle, and small real parts appear in the characteristic exponents, causing the solution (8) to become unstable. The dissolution of the system (the escape of the test particle from L_4) is slower near the boundary of the stable domain, and speeds up with the increase of the positive real parts of the characteristic exponents. This is in good agreement with the escape times from L_4, computed in Érdi et al. (2009).

In Fig. 2 of Érdi et al. (2009), the unstable region is divided into two parts by a dim boundary, along which the lifetime of the system (until the test particle remains in the vicinity of L_4) slightly increases. The authors suspected that the boundary between the U2 and U3 domains is responsible for this. Here, in Fig. 2, we show the escape time of the test particle (on a logarithmic scale) as a function of μ, for several

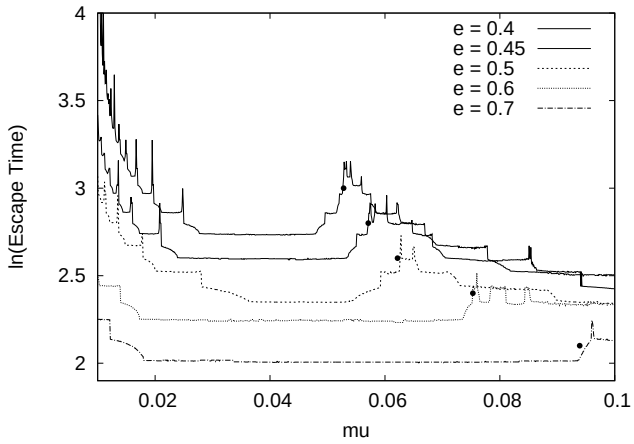

Figure 2. The escape time of the test particle from L_4 (on a logarithmic scale) depending on μ, for several values of $e \geqslant 0.4$. (We note that for $e > 0.3143$ L_4 is unstable for most values of μ, see Fig. 1.) Black dots mark the boundary points between the U2 and U3 domains of Fig. 1 for the same values of e.

values of e, determined by Rajnai, Nagy & Érdi (2010). For the same values of e, the points of the boundary between the U2 and U3 domains of Fig. 1 are also marked (black dots). It can be seen that these boundary points fit well to the places of the slight local increase of the escape time. As we shall see in Section 5, this boundary corresponds to several 1:1 resonances, making resonances accountable for the small growth in the escape time.

3.2 Characteristic exponents

The real parts of the characteristic exponents ν_j in (7) are responsible for the exponential escape of the test particle from L_4, while the imaginary parts in (7) result in periodic motion of infinitesimal amplitude around L_4 with frequencies

$$n_j = \frac{\varphi_j + k2\pi}{T}. \tag{9}$$

Considering that ν_j occur in complex conjugate pairs (similarly to the complex characteristic roots λ_j), and that in the ERTBP there are 4 frequencies of libration around L_4 (Rabe 1973; Érdi et al. 2007), we specified $k = 0, 1$ in (9). Thus with $T = 2\pi$, the 4 frequencies in the ERTBP are n_s, n_l, $1-n_s$, and $1-n_l$, where n_s and n_l are the frequencies of the short and long period libration around L_4, while $1-n_s$ and $1-n_l$ are due to the elliptic motion of the Lagrangian point L_4 itself.

Fig. 3 shows the real parts and the frequencies corresponding to the imaginary parts of the characteristic exponents, depending on μ, for several values of e.

The panel (a) displays the real parts (gray curves) and the fequencies (black curves) for the limit case $e = 0$. For $\mu < 0.03852$, there are 4 frequencies, n_s, n_l, $1-n_s$, $1-n_l$. The point A marks the place, where the frequencies n_l and $1-n_l$ become equal ($n_l = 0.5$). This occurs at $\mu = 0.02859$, at the critical point A of the stability domain in Fig. 1. The point A is the starting point of the A11 type resonance for $e > 0$, as it will be seen in Section 5. Similarly, the points B and C are the starting points of the B11 and C11 resonances,

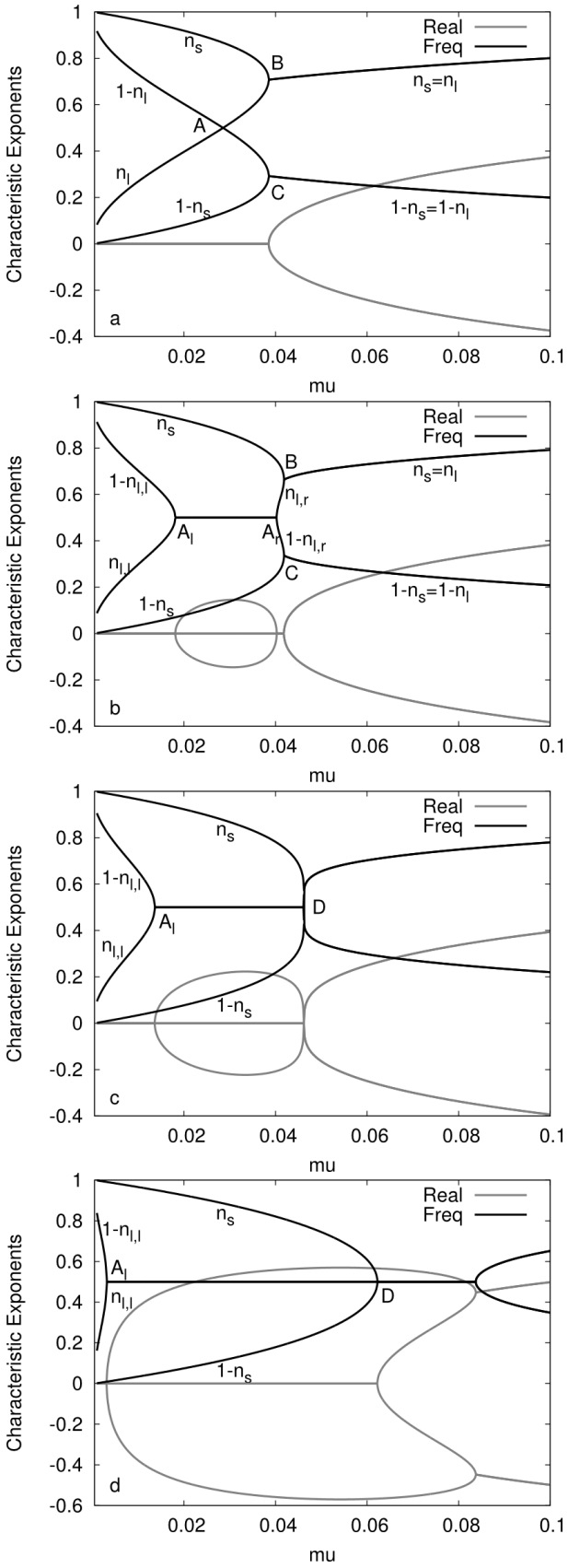

Figure 3. The real parts and the frequencies corresponding to the imaginary parts of the characteristic exponents, depending on μ, for several values of e: panel (a) $e = 0$; (b) $e = 0.2$; (c) $e = 0.3$; (d) $e = 0.65$.

where $n_s = n_l$ and $1-n_l = 1-n_s$, respectively. These points occur at $\mu = 0.03852$, corresponding to the point B of the stability domain in Fig. 1.

The difference of the present work from earlier ones (Danby 1964; Bennett 1965; Érdi et al. 2007) is, that from the characteristic exponents we computed the frequencies in such domains of the μ, e plane, where they were not considered before. Thus increasing the mass parameter over $\mu = 0.03852$, in the unstable domain the frequencies remain equal in pairs, $n_s = n_l$ and $1 - n_l = 1 - n_s$ (Fig. 3a), and instead of the so-far zero real parts in the stable domain ($\mu < 0.03852$), 2 non zero real parts appear, causing the test particle to escape from L_4.

Increasing the eccentricity, the point A of Fig. 3a splits into two, as can be seen in Fig. 3b for $e = 0.2$ (A_l on the left, A_r on the right). For values of μ between A_l and A_r, there are two complex and two imaginary characteristic exponents (see the bottom panel of Fig. 1). The frequencies corresponding to the imaginary parts of the 2 complex characteristic exponents are equal, $n_l = 1 - n_l = 0.5$, and can be seen between A_l and A_r (Fig. 3b).

To the 2 imaginary characteristic exponents there correspond the n_s and $1 - n_s$ frequencies. For values of μ in the stability region, on the left from A_l and on the right from A_r there are 4 frequencies, corresponding to the 4 imaginary characteristic exponents. In the unstable domain ($\mu > 0.03852$), $n_s = n_l$ and $1 - n_l = 1 - n_s$, as in Fig. 3a. The properties of the real parts are similar to those of Fig. 3a, and two more real parts appear for values of μ between A_l and A_r, corresponding to the two complex characteristic exponents in this domain (see the bottom panel of Fig. 1).

Increasing further the eccentricity, the points A_l and A_r move in opposite derection, B and C move toward each other, and finally for $e = 0.3143$ and $\mu = 0.04698$ the three points A_r, B, and C are united in one point, marked by the letter D in Fig. 3c, and corresponding to the upper right peak D of the stability domain in Fig. 1, where all 4 frequencies become equal. Afterwards, the properties of the frequencies, and that of the real parts in the whole domain of μ are similar to as in Fig. 3b.

In Fig. 3d one can see the frequencies for $e = 0.65$. Here D corresponds to that point, where in the upper panel of Fig. 1 the $e = 0.65$ line would cross the border between the U1 and U3 domains. All frequencies are equal from the point D until another point which would correspond to the intersection of the $e = 0.65$ line and the border of the U2 and U3 domains. From this point on, two pairs of equal frequencies exist. For larger values of μ ($0.1 < \mu < 0.5$), the properties of the frequencies and the real parts are similar to as in Fig. 3d.

We note that for a given eccentricity, the real parts of the characteristic exponents change very steeply near the border of the stability regions S1 and S2 (see Figs 3b, c, d for values of μ corresponding to the point A_l, for example), and the abrupt changes in the positive real parts result in shorter escape times at the border of the stable region.

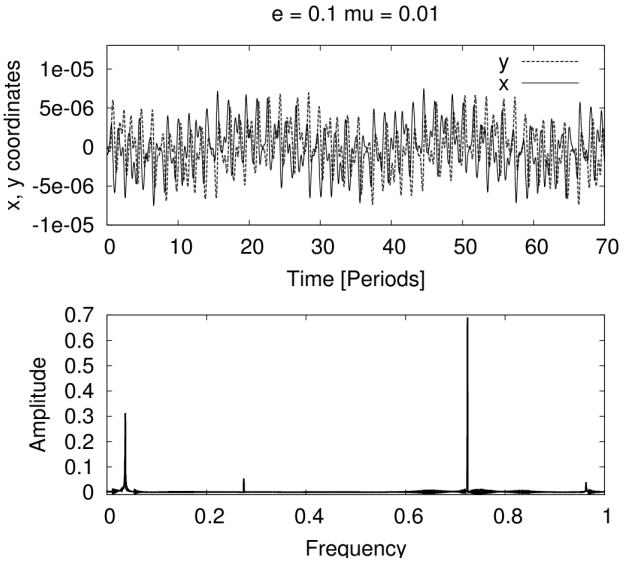

Figure 4. Top panel: Variation of the x and y coordinates of the test particle relative to L_4 with time for $e = 0.1$, $\mu = 0.01$, and initial conditions described in the text. Bottom panel: Fourier spectrum of the motion shown in the top panel.

4 FREQUENCIES

4.1 A comparison of the frequencies

In Section 3.2 we determined the frequencies of motion around L_4 by using Floquet's theory. For comparison, we also computed the frequencies by the method of fast Fourier transform (FFT).

For this we integrated the equations of motion of the ERTBP numerically, over 1250 periods of the primaries (this proved to be a long enough time interval), by changing e and μ on the same grid as in Section 2.3. The test particle was given a 10^{-6} displacement from L_4 in the x direction as initial condition (and zero initial velocity in the rotating coordinate system).

The top panel of Fig. 4 shows the x and y coordinates of the test particle relative to L_4 for $e = 0.1$, and $\mu = 0.01$. Periodicities are well recognizable in both coordinates, the motion of the test particle is stable for this value of e and μ. Applying FFT on the time series of the coordinates, Fourier spectra can be determined on which 4 peaks, corresponding to the 4 frequencies of motion around L_4, can be identified (bottom panel of Fig. 4).

FFT performed well in the stable domain (S1 and S2), but in the unstable region (U1) the lifetime of the system was too short to get usable spectra. The decay of the system was due to escape or collision of the test particle with either of the primaries. In the former case exponential runaway dominated the motion, so the spectrum also. These effects are responsible for the missing FFT data in Fig. 5, where comparison of the two methods, FFT and Floquet's theory can be seen for $e = 0.1$. For this value of e, L_4 is unstable between $0.021 < \mu < 0.033$ (see Fig. 1), and there are 2 imaginary and 2 complex characteristic exponents. To the imaginary exponents there correspond periodic motions, however their frequencies could not be determined by FFT for the aforementioned reasons. According to Fig. 5, the agreement between the results of the two methods are good, and where

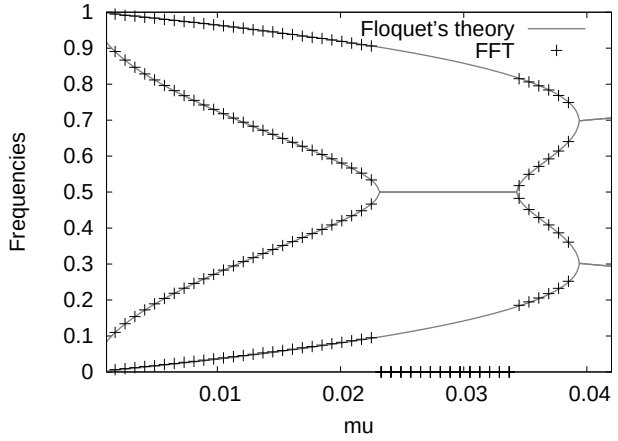

Figure 5. Comparison of the frequencies determined by using FFT (marked by cross), and Floquet's theory (solid lines) for $e = 0.1$. Between $0.021 < \mu < 0.033$ the frequencies refer to the unstable region U1.

FFT could not work, the application of Floquet's theory could provide the frequencies.

4.2 Fitting the frequencies

In Section 3.2 we determined the frequencies by using Floquet's theory. Fig. 3 shows these frequencies for several values of e as the function of μ. In the limit case $e = 0$, the n_s, n_l frequencies in the stable domain $0 < \mu < 0.03852$ can also be computed from the well-known equations (Érdi et al. 2009)

$$n_s = \sqrt{|-0.5 - 0.5\sqrt{27(\mu - 0.5)^2 - 5.75}|},$$
$$n_l = \sqrt{|-0.5 + 0.5\sqrt{27(\mu - 0.5)^2 - 5.75}|}. \quad (10)$$

Comparing the top and middle panels of Fig. 3, it can be seen that the frequencies are changing with the increase of the eccentricity, however, the character of the curves remains. This gives the idea of searching for fitting functions of the frequency curves in the form of Eq. (10). Due to the symmetry of the curves, it is enough to fit those parts of the curves which correspond to the n_s and n_l frequencies. From these the fit for the $1 - n_s$, $1 - n_l$ frequencies is immediately obtained.

The n_s curve remains continuous as the eccentricity is increasing, but the n_l curve has a breakpoint at $\mu = 0.02859$, marked by a letter A in Fig. 3a. Increasing e above 0, the point A splits to two points (A_l and A_r in Fig. 3b). Thus the n_l curve also splits to a left $n_{l,l}$ and a right $n_{l,r}$ side.

(Between A_l and A_r, $n_l = 1 - n_l = 0.5$ as we have seen in Section 3.2.) Therefore, we fitted the $n_{l,l}$ and $n_{l,r}$ curves separately. Denoting the μ coordinates of the A_l and A_r points by μ_l and μ_r, respectively, we fitted the $n_{l,l}$ curve in the interval $0 < \mu < \mu_l$, and the $n_{l,r}$ curve in $\mu_r < \mu < 0.04698$. For a given value of e, these are the two domains in μ where L_4 is stable. In the Appendix, we give the equations from which μ_l and μ_r can be computed for a given value of e.

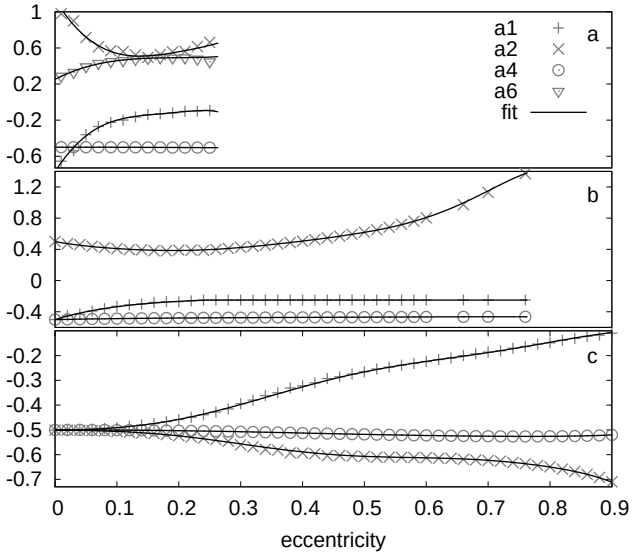

Figure 6. The a_i parameters depending on the eccentricity for the frequencies $n_{l,r}$ (a); $n_{l,l}$ (b); and n_s (c) panel. Grey crosses, x-es, circles, and triangles indicate the determined parameter values for the given eccentricity, while the black solid lines mark the fitted polynomial functions.

We assumed the fitting functions for the n_s, $n_{l,l}$, and $n_{l,r}$ curves in the form

$$f(\mu) = a_0\sqrt{|a_1 + a_2\sqrt{a_3(\mu + a_4)^2 + a_5}|} + a_6, \quad (11)$$

by allowing the dependence of the fitting parameters a_i on the eccentricity, $a_i = a_i(e)$. However, we got the best fits by keeping $a_3 = 27.0$, $a_5 = -5.75$ for each frequency; $a_0 = 1.0$, $a_6 = 0.0$ for n_s and $n_{l,l}$; and $a_0 = 0.5$ for $n_{l,r}$, independent of e. The remaining parameters showed dependence on e. These parameters were determined in the following way.

We computed the n_s, $n_{l,l}$, $n_{l,r}$ frequency curves for different values of e by using Floquet's theory, and fitted them by the functions (11). Fig. 6 shows the computed a_i coefficients depending on e (except the fixed ones, which do not depend on e). Fig. 6a refers to the $n_{l,r}$ curves in the domain $0 < e < 0.3143$, $\mu_r < \mu < 0.04698$. The upper limits correspond to the upper right peak of the stability region (point D in Fig. 1). We note that near this peak the number of the determined frequencies were too low for an efficient fit. Fig. 6b shows the coefficients for the $n_{l,l}$ curves in the domain $0 < e < 0.75$, $0 < \mu < \mu_l$. (Due to the fast changes in the n_l frequency for large values of e we could determine the fitting coefficints only up to $e \sim 0.75$.) In Fig. 6c, the coefficients for the n_s curves can be seen for $0 < e < 0.9$, $0 < \mu < 0.0633$.

Next we fitted the computed a_i coefficients with polynomial functions of the eccentricity

$$a_i(e) = \sum_j a_{i,j} \cdot e^j,$$

except a_1 for the $n_{l,l}$ curve, where we used an exponential fitting function (based on several trials searching for the best representation). In Fig. 6 the black solid lines mark the

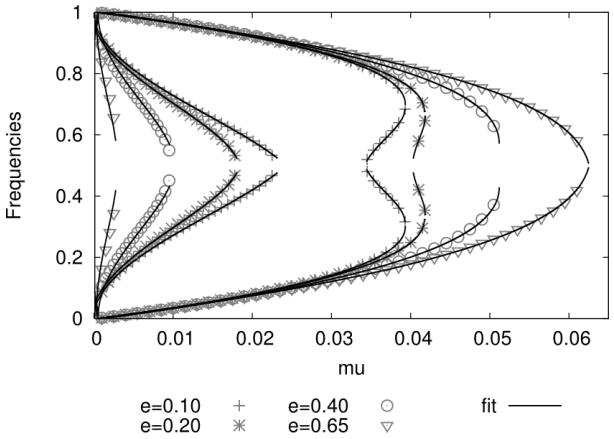

Figure 7. Grey symbols mark the the frequencies computed by using Floquet's theory, and solid black lines stand for frequencies obtained from equation (11), after fitting the parameters. The $n_l = 1 - n_l = 0.5$ frequencies are not shown for clarity of the figure.

fitted polynomial functions, whose $a_{i,j}$ coefficients are given in the Appendix.

Fig. 7 shows the frequencies computed by using Floquet's theory for several eccentricities (marked by different symbols), and obtained from the fitting functions (11) with the determined coefficients (black solid lines). The accuracy of the fit of the n_l curves decreases at the border (at the A_l, A_r points, see Fig. 3b) and near the upper right peak point D of the stability domain, due to the rapid changing of the frequency and the low number of the fitted data. However, farther from these places, the fit agrees well with the computed frequencies.

5 RESONANCES

Érdi et al. (2007) determined the size distribution of the stable regions of motions around L_4 in the μ, e plane and found that there are minimum zones, whose places can be related to resonances between the 4 frequencies of libration in the ERTBP. The possible resonances are defined in Érdi et al. (2007) and listed in Table 1.

By computing the frequencies via Floquet's theory, we could map the resonances on the μ, e plane. The results are shown in Figs 8 and 9. These extends the results of previous investigations (Érdi et al. 2007, 2009). For a better visualization, we mapped the reciprocal of the frequency ratios given in Table 1. Thus the A type 1:2 resonance in the top panel of Fig. 8 corresponds to the A type 2:1 resonance in Érdi et al. (2007). Fig. 8 shows the frequency ratios of the types A, B, and C, and Fig. 9 the same for the types D, E, and F, with some highlighted resonance curves.

The extended white domain in each panel indicates the positions of 1:1 resonances, where the frequencies become equal. This occurs not only along narrow curves as expected before, but in very extended regions which cover large parts of the μ, e plane, and follow the boundaries shown in Fig. 1. The 1:1 resonance of type A (hereafter A11) corresponds to that region in the μ, e plane, where at least 2 real characteristic roots appear with negative sign (U1 and U3 regions in

Table 1. Types of resonances

A	$(1 - n_l)$	:	n_l
B	n_s	:	n_l
C	$(1 - n_l)$	:	$(1 - n_s)$
D	n_s	:	$(1 - n_l)$
E	n_s	:	$(1 - n_s)$
F	n_l	:	$(1 - n_s)$

Fig. 1). The negative real characteristic roots result in frequencies, through the characteristic exponents, equal to 0.5, and these frequencies are the n_l, and $1 - n_l$ fequencies, corresponding to the A type resonance. This can also be seen in Fig. 3.

The 1:1 resonance of types B and C (B11 and C11) covers the unified domain of U2 and U3 of Fig. 1, where there are 4 complex characteristic exponents. The 1:1 resonances appear due to the fact that the imaginary parts of the characteristic exponents are equal in pairs. In those regions of the μ, e plane, where 4 negative real characteristic roots are possible (U1, U2, and U3 in Fig. 1), the imaginary parts of the characteristic exponents are all equal to -0.5. Thus in these regions we expect A11, B11, C11, D11, E11, and F11 resonances, and the maps of Figs 8 and 9 actually show this. One can see that $1 : 1$ resonances cover the whole unstable domain of the μ, e parameter plane, suggesting that they can be responsible in a large measure for the loss of stability of the point L_4 in the ERTBP.

It can be seen from Fig. 9 that for those values of μ and e

which correspond to the U2 domain, the D, E, and F resonances have the same character. The reason for this is that in the U2 domain there are also B11 and C11 resonances, meaning that $n_s = n_l$, and $1 - n_l = 1 - n_s$, and it follows (see Table 1) that D=E=F. Moreover, these resonances are also equal to 1/A (compare the A 3:1 and D, E, F 1:3 resonances in Figs 8 and 9).

The resonance curves of the A, B, and D types in the S1 and S2 stability domains

are in good agreement with the results obtained in Érdi et al. (2007) by using Rabe's equation (Rabe 1973), and the A and E type resonances agree with those determined in Kovács (2013) by using the energy-rate method (the E type resonance was computed in both the stable and unstable domains). We note that the C and F type resonance curves show peculiar shapes in the stable domain. This is in connection with the phenomenon that resonance curves do not behave regulary on the boundary of the stability region. Crossing the boundary they break, making difficult to find a good fitting function. The most striking examples can be seen in the cases of the C and F type resonances in Figs 8 and 9.

We know from stability investigations of the Solar system that resonances can protect, but can also destroy systems of celestial bodies. Kovács (2013) suggested that resonances can be responsible for longer escape times of the test particle in the unstable domains of the μ, e plane. We checked if the peaks in the escape time of the test particle (see Fig. 10) could be in connection with some resonances.

Fig. 10 shows the changing of the escape time of the test particle depending on μ for $e = 0.4$ and 0.45. Several

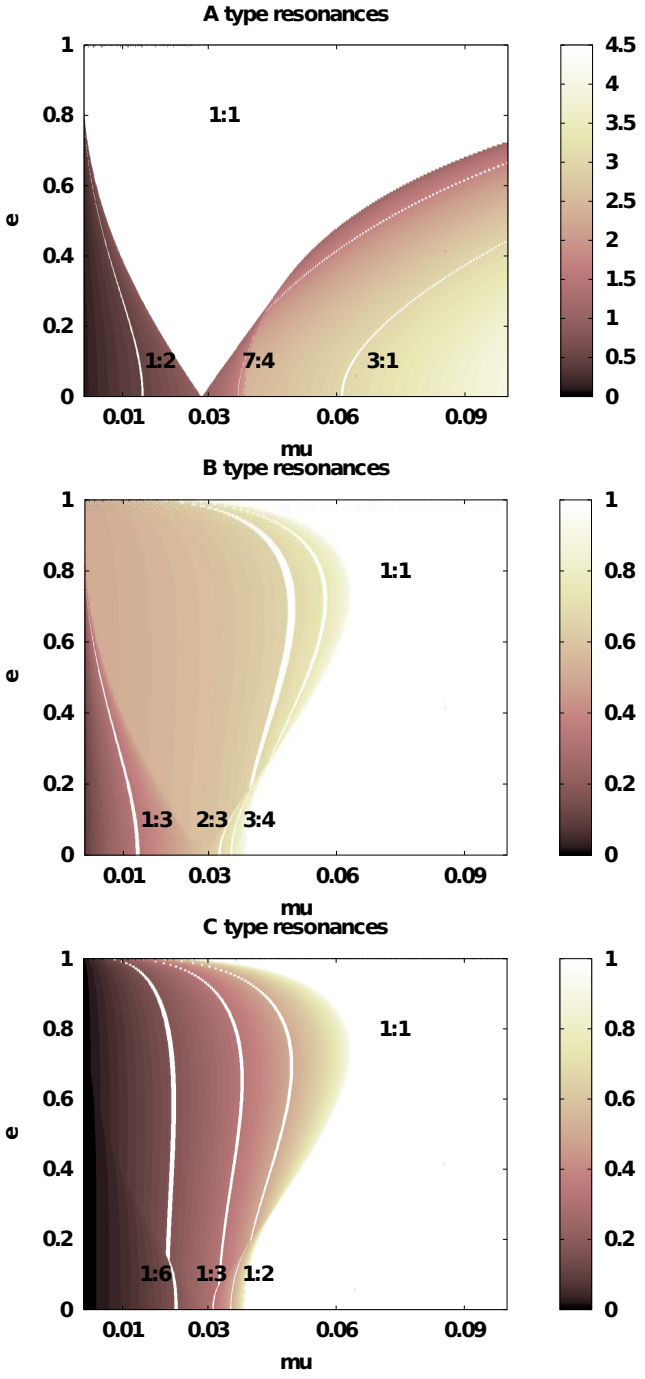

Figure 8. Maps for the A, B, and C types of resonances. The colorbar indicates the continuous change of the reciprocal of the frequency ratios on the μ, e plane. The white curves indicate a few resonances between the frequencies. The extended white domain in each panel stays for 1:1 resonances, where the frequencies are equal.

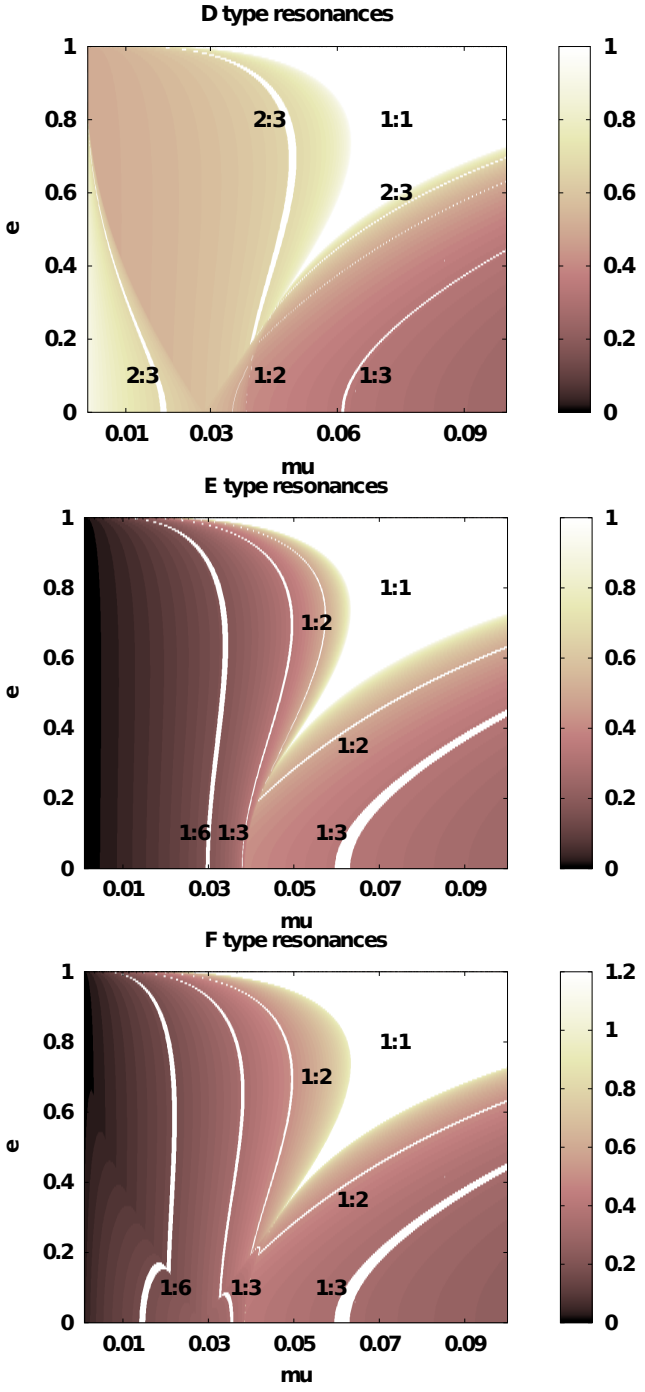

Figure 9. Maps for the D, E, and F types of resonances. For further details see the caption of Fig. 8.

peaks of the escape time curves can be identified with resonances. Among these protective resonances there are low order (2:3, 2:5, 4:5), and high order (25:49, 1:11, 1:21) resonances as well. There are also many multiple resonances, corresponding to different types at the same time (like 9:10, 7:11 referring to A, D, E, and F types).

An interesting behaviour is that by changing the eccentricity, protective resonances can become destroying ones, decreasing the escape time of the test particle. For example, for $e = 0.4$ the C 1:11, E 1:21, F 1:21, and 4:5 resonances are protective, but for $e = 0.45$ they are destroying to which there correspond pits in the escape time curve in Fig. 10.

6 SUMMARY

By using Floquet's theory (Floquet 1883) and following the methods described by Danby (1964) and Bennett (1965), we

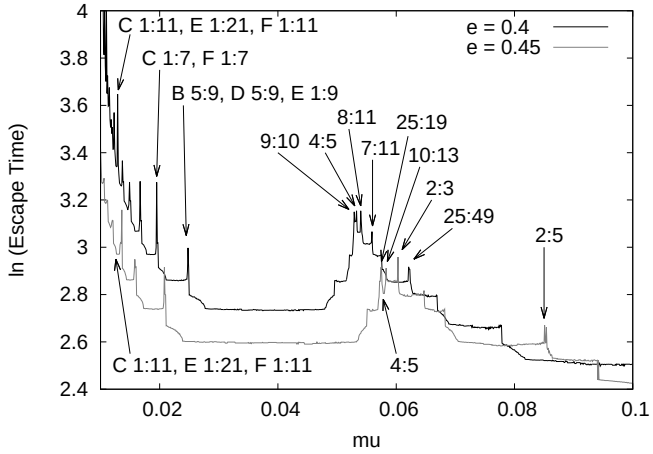

Figure 10. Resonances corresponding to longer escape times of the test particle in the unstable domains for $e = 0.4$ and 0.45. Resonances without the letter of the type refer to A, D, E, and F multiple resonances. For example, 4:5 means A 5:4, D 4:5, E 4:5, and F 4:5 resonances.

computed the characteristic roots and characteristic exponents of infinitesimal motion around the Lagrangian point L_4 in the elliptic restricted three-body problem for the domains of the mass parameter $0 < \mu \leqslant 0.5$ and eccentricity $0 \leqslant e < 1$. We numerically integrated the first variational equations of motion around L_4 to build up the fundamental matrix, from its eigenvalues we determined the characteristic roots and exponents, and from the latters the frequencies of the periodic components of motions depending on μ and e. According to the properties of the characteristic roots, we distinguished stable and unstable domains of L_4 in the μ, e plane in agreement with former results (Danby 1964; Bennett 1965) .

We computed the frequencies not only in the stable domains, but also in the unstable regions. We also determined frequencies by the method of fast Fourier transform. The results obtained by the two methods are in good agreement, but the method based on Floquet's theory were applicable in such regions of the μ, e plane, where FFT did not work (due to short data sets as a consequence of fast escape of the test particle).

We studied how the librational frequencies in the stable domain depend on the mass parameter and the eccentricity. Based on the frequency - mass parameter relationship of the circular restrictd three-body problem, we determined fitting functions for the frequencies in the ERTBP which give the frequencies depending on μ and e. These are given in the Appendix.

Between the 4 frequencies of motion around L_4 in the ERTBP, there can be 6 types of resonances (Érdi et al. 2007, 2009). We studied the frequency ratios in the whole investigated μ, e plane. We found that 1:1 resonances occur not only along narrow curves, but in very extended regions, and different types of 1:1 resonances cover the whole unstable region in the μ, e plane. Different types of resonances correspond to different types of characteristic roots and characteristic exponents in the μ, e plane.

The escape time of the test particle in the unstable domain, depending on μ and e, can also be related to resonances. There are protective resonances, where the escape times are longer at the corresponding values of μ and e. These resonances can be responsible for the longer escape times of the test particle from L_4. However, by changing the parameters (e for a given μ) the character of the resonance may change resulting in shorter escape time of the test particle.

ACKNOWLEDGMENTS

REFERENCES

Bennett A., 1965, Icarus, 4, 177
Danby J.M.A., 1964, AJ, 69, 2
Érdi B., Nagy I., Sándor Zs., Süli Á., Frölich G., 2007, MNRAS, 381, 33
Érdi B., Forgács-Dajka E., Nagy I., Rajnai R., 2009, Celest. Mech. & Dyn. Astr., 104, 145
Floquet G., 1883, Annales de l'École Normale Supérieure 12, 47
Kovács T., 2013, MNRAS, 430, 2755
Lohinger E., Dvorak R., 1993, AA, 280, 683
Markellos V.V., Papadakis K.E., Perdios E.A., 1995, in Roy A.E., Steves B., eds, From Newton to Chaos. Plenum Press, New York, p. 371
Meire R., 1981, Celest. Mech., 23, 89
Rabe E., 1973, in Tapley E.D., Szebehely V., eds, Recent Advances in Dynamical Astronomy. D. Reidel Publ. Co., Dortrecht, p. 155
Rajnai R., Nagy I., Érdi B., 2010, J. Phys. Conf. Ser., 218, 012018
Schwarz R., Bazsó Á., Érdi B., Funk B., 2012 MNRAS, 427, 397
Tschauner J., 1971, Celest. Mech., 3, 189
Szebehely V., 1967, Theory of Orbits. Academic Press, New York

APPENDIX A: FITTING THE FREQUENCIES

The n_l curve is separated to two sides, $n_{l,l}$ and $n_{l,r}$, and two different parameter sets were used for their fit. Between the two sides, n_l is constant, $n_l = 0.5$. The μ_l and μ_r coordinates of the breakpoints of the n_l curve for given values of e can be computed from the polynomial functions given in Érdi et al. (2009):

$$\mu_l = 0.0285955 - 0.0555801e + 0.0090947e^2 + 0.0341118e^3 - 0.0163862e^4,$$

$$\mu_r = 0.0285955 + 0.0577951e + 0.0026645e^2 + 0.0234761e^3 - 0.0750853e^4.$$

The fitting functions for the frequencies are (changing the notations of Section 4.2 for convenience, and keeping only the fitted coefficients)

$$n_s(\mu) = \sqrt{|A_1 + A_2\sqrt{27(\mu + A_3)^2 - 5.75}|} \qquad \text{(A1)}$$

$$n_l(\mu) = \begin{cases} \sqrt{|B_1 + B_2\sqrt{27(\mu+B_3)^2 - 5.75}|} \\ \quad \text{if } \mu < \mu_l \\ 0.5 \quad \text{if } \mu_l < \mu < \mu_r \\ 0.5\sqrt{|C_1 + C_2\sqrt{27(\mu+C_3)^2 - 5.75}|} + C_4 \\ \quad \text{if } \mu > \mu_r \end{cases} \quad \text{(A2)}$$

where the A_i, B_i, C_i coefficients are polynomials of the eccentricity

$$A_i(e) = \sum_j a_{i,j} \cdot e^j,\ B_i(e) = \sum_j b_{i,j} \cdot e^j,\ C_i(e) = \sum_j c_{i,j} \cdot e^j,$$

except B_1, where we used an exponential fitting function: $B_1 = b_{1,1} \exp(b_{1,2}\, e) + b_{1,3}$.

A1 Fitting parameters for $\mathbf{n_s}$

$$n_s(\mu) = \sqrt{|A_1 + A_2\sqrt{27(\mu+A_3)^2 - 5.75}|} \quad \text{(A3)}$$

$$\begin{aligned} A_1 &= a_{1,1} + a_{1,2}e + a_{1,3}e^2 + a_{1,4}e^3 + a_{1,5}e^4 + a_{1,6}e^5 + \\ &\quad + a_{1,7}e^6 + a_{1,8}e^7 + a_{1,9}e^8 \\ A_2 &= a_{2,1} + a_{2,2}e + a_{2,3}e^2 + a_{2,4}e^3 + a_{2,5}e^4 + a_{2,6}e^5 + \\ &\quad + a_{2,7}e^6 + a_{2,8}e^7 + a_{2,9}e^8 \\ A_3 &= a_{3,1} + a_{3,2}e + a_{3,3}e^2 + a_{3,4}e^3 + a_{3,5}e^4 + a_{3,6}e^5 + \\ &\quad + a_{3,7}e^6 + a_{3,8}e^7 \end{aligned} \quad \text{(A4)}$$

$$\begin{aligned} a_{1,1} &= -0.501002169796915 \\ a_{1,2} &= -0.00465201800792375 \\ a_{1,3} &= 1.39021245993088 \\ a_{1,4} &= -7.65704222733915 \\ a_{1,5} &= 58.9694647229867 \\ a_{1,6} &= -184.999091047886 \\ a_{1,7} &= 268.30016373139 \\ a_{1,8} &= -184.282471189398 \\ a_{1,9} &= 48.6925607416981 \end{aligned}$$

$$\begin{aligned} a_{2,1} &= -0.500999575602288 \\ a_{2,2} &= 0.0037393921033813 \\ a_{2,3} &= -0.883321850087518 \\ a_{2,4} &= 7.55148105681823 \\ a_{2,5} &= -59.917802755943 \\ a_{2,6} &= 200.631458043772 \\ a_{2,7} &= -317.115523217342 \\ a_{2,8} &= 240.11269595431 \\ a_{2,9} &= -70.8037648777467 \end{aligned} \quad \text{(A5)}$$

$$\begin{aligned} a_{3,1} &= -0.499999914619729 \\ a_{3,2} &= -0.000238236951561991 \\ a_{3,3} &= -0.0864876445889037 \\ a_{3,4} &= 0.190520373359826 \\ a_{3,5} &= -1.35033175168857 \\ a_{3,6} &= 3.62324711720567 \\ a_{3,7} &= -3.8958192249963 \\ a_{3,8} &= 1.52170604628458 \end{aligned}$$

A2 Fitting parameters for $\mathbf{n_{l,l}}$

$$n_{l,l}(\mu) = \sqrt{|B_1 + B_2\sqrt{27(\mu+B_3)^2 - 5.75}|} \quad \text{(A6)}$$

$$\begin{aligned} B_1 &= b_{1,1} \exp(b_{1,2}e) + b_{1,3} \\ B_2 &= b_{2,1} + b_{2,2}e + b_{2,3}e^2 + b_{2,4}e^3 + b_{2,5}e^4 + b_{2,6}e^5 + \\ &\quad + b_{2,7}e^6 + b_{2,8}e^7 \\ B_3 &= b_{3,1} + b_{3,2}e + b_{3,3}e^2 + b_{3,4}e^3 + b_{3,5}e^4 \end{aligned} \quad \text{(A7)}$$

$$\begin{aligned} b_{1,1} &= -0.283143803539808 \\ b_{1,2} &= -8.80063684576695 \\ b_{1,3} &= -0.217255471020594 \end{aligned}$$

$$\begin{aligned} b_{2,1} &= 0.50036132088182 \\ b_{2,2} &= -1.50595975540227 \\ b_{2,3} &= 10.115844050892 \\ b_{2,4} &= -63.0931155920938 \\ b_{2,5} &= 285.264900151338 \\ b_{2,6} &= -666.727927110675 \\ b_{2,7} &= 752.16230243293 \\ b_{2,8} &= -322.241229133452 \end{aligned} \quad \text{(A8)}$$

$$\begin{aligned} b_{3,1} &= -0.499930735128903 \\ b_{3,2} &= 0.15970524654665 \\ b_{3,3} &= -0.398529593818837 \\ b_{3,4} &= 0.561419591971936 \\ b_{3,5} &= -0.303312424339199 \end{aligned}$$

A3 Fitting parameters for $\mathbf{n_{l,r}}$

$$n_{l,r}(\mu) = 0.5\sqrt{|C_1 + C_2\sqrt{27(\mu+C_3)^2 - 5.75}|} + C_4 \quad \text{(A9)}$$

$$\begin{aligned} C_1 &= c_{1,1} + c_{1,2}e + c_{1,3}e^2 + c_{1,4}e^3 + c_{1,5}e^4 + c_{1,6}e^5 \\ C_2 &= c_{2,1} + c_{2,2}e + c_{2,3}e^2 + c_{2,4}e^3 \\ C_3 &= c_{3,1} + c_{3,3}e^2 \\ C_4 &= c_{4,1} + c_{4,2}e + c_{4,3}e^2 + c_{4,4}e^3 \end{aligned} \quad \text{(A10)}$$

$$\begin{aligned} c_{1,1} &= -0.769762964976643 \\ c_{1,2} &= 10.5612231908263 \\ c_{1,3} &= -54.5231687808546 \\ c_{1,4} &= -10.8373555491553 \\ c_{1,5} &= 892.817398534855 \\ c_{1,6} &= -1921.57814251696 \end{aligned}$$

$$\begin{aligned} c_{2,1} &= 1.13820612112604 \\ c_{2,2} &= -11.2718231877969 \\ c_{2,3} &= 64.2577426648982 \\ c_{2,4} &= -113.455649510537 \end{aligned} \quad \text{(A11)}$$

$$\begin{aligned} c_{3,1} &= -0.499867875893531 \\ c_{3,3} &= -0.0859479289026476 \end{aligned}$$

$$\begin{aligned} c_{4,1} &= 0.252209443579731 \\ c_{4,2} &= 3.53516545799185 \\ c_{4,3} &= -17.6970689361691 \\ c_{4,4} &= 30.0317028979599 \end{aligned}$$

This paper has been typeset from a TEX/ LATEX file prepared by the author.